Published in final edited form as:

Dev Dyn. 2020 May ; 249(5): 666–678. doi:10.1002/dvdy.154.

Annexin A3 is necessary for parallel artery-vein alignment in the mouse retina

Katie Huang[#1], **Angela M. Crist**[#1], **Nehal R. Patel**[1], **Avery Blanks**[1], **Kelsey Carter**[2], **Ondine Cleaver**[2], **Stryder M. Meadows**[1]

[1]Cell and Molecular Biology Department, Tulane University, New Orleans, Louisiana

[2]Department of Molecular Biology, University of Texas Southwestern Medical Center, Dallas, Texas

[#] These authors contributed equally to this work.

Abstract

Background: Annexin A3 (Anxa3) is a member of the calcium-regulated, cell membrane-binding family of annexin proteins. We previously confirmed that Anxa3 is expressed in the endothelial lineage in vertebrates and that loss of *anxa3* in *Xenopus laevis* leads to embryonic blood vessel defects. However, the biological function of Anxa3 in mammals is completely unknown. In order to investigate Anxa3 vascular function in mammals, we generated an endothelial cell-specific *Anxa3* conditional knockout mouse model (*Anxa3*$^{f/f}$;*Tie2*-Cre).

Results: *Anxa3*$^{f/f}$;*Tie2*-Cre mice are born at Mendelian ratios and display morphologically normal blood vessels during development. However, loss of *Anxa3* leads to artery-vein (AV) misalignment characterized by atypical AV crossovers in the postnatal and adult retina.

Conclusions: *Anxa3* is not essential for embryonic blood vessel formation but is required for proper parallel AV alignment in the murine retina. AV crossovers associated with *Anxa3*$^{f/f}$;*Tie2*-Cre mice are similar to AV intersections observed in patients with branch retinal vein occlusion (BRVO), although we did not observe occluded vessels. This new *Anxa3* mouse model may provide a basis for understanding AV crossover formation associated with BRVO.

Keywords

annexin; artery; development; mouse; patterning; retina; vascular; vein

1 | INTRODUCTION

Annexins are a family of 12 calcium-dependent phospholipid-binding proteins named annexins A1-A12 (Anxa1-12). Each family member has a short, unique N-terminal domain

Correspondence Stryder M. Meadows, Tulane University, Cell and Molecular Biology Department, 6400 Freret St., 2000 Percival Stern Hall, New Orleans, LA 70118. smeadows@tulane.edu.

AUTHOR CONTRIBUTIONS

K.H., A.M.C., and S.M.M. developed experiments. K.H., N.P., A.B., and K.C. performed genotyping, immunofluorescent staining, *in situ* hybridizations and quantification. S.M.M. performed quantifications. K.H., N.P., A.B., K.C., and A.M.C. performed retinal dissections. A.M.C. performed next generation sequencing experiments and *in situ* hybridizations. A.M.C. and S.M.M. wrote the article.

that is thought to interact with various cytosolic proteins. The remaining annexin protein predominately consists of an “annexin” core, which is comprised of annexin repeat domains that utilize Ca^{2+} to bind to the negatively charged phospholipids of the cell membrane.[1] Typically, this Ca^{2+}-phospholipid interaction occurs at the inner cell membrane; however, additional evidence indicates that annexins are also present and function on the outer cell membrane.[1,2] Due to the nature of annexins’ interactions with the phospholipid bilayer, these proteins aid in membrane-membrane or membrane-cytoskeleton communication, and are subsequently involved in a variety of processes, including endocytosis, exocytosis, membrane organization, cellular migration, inflammation, viral production, and fibrinolysis.[1,3–9]

Members of the annexin family are expressed in a wide variety of vertebrate tissues; however, in context of the cardiovascular system, only a subset of annexin family members has exhibited expression in the endothelium. For instance, Anxal, 2, 3, 5, 6, and 11 are expressed in endothelial cells (ECs) of human, mouse, chicken, frog, and zebra fish tissues.[10–18] Interestingly, higher vertebrates, such as mice, express a number of annexins in the embryonic EC lineage, including *Anxa2, 3, 5,* and *6*.[11,13,16–18] In contrast, lower vertebrates appear to express fewer annexins in the endothelium: only *anxa2* and 3 have been detected in the EC lineage of frogs,[16] while in zebra fish, only *anxa3* has been shown to be expressed in ECs.[12,16] Thus, expression studies suggest that *anxa2* and *3* might have core, evolutionary embedded roles in vascular biology. Indeed, a number of *in vitro* and *in vivo* studies have established a functional role for Anxa2 in various vascular processes. *Anxa2* knockout mice display defects in fibrin clearance from blood vessel clots and a reduction in neovascularization.[13,19,20] Furthermore, experiments in cultured primary ECs have demonstrated that Anxa2 is involved in the process of von Willebrand Factor (vWF) secretion from Weibel-Palade bodies[21,22] and in EC junctional stability.[23–25]

In contrast, the role of Anxa3 in the endothelium is less understood and has mostly been defined by *in vitro* experiments. Park et al. (2005) first implicated *ANXA3* in EC migration and tube formation in human umbilical vein endothelial cells (HUVECs). Conditioned media from HEK 293 cells overexpressing ANXA3 were able to induce migration of HUVEC in a chemotaxis chamber.[26] This media exhibited an increase in vascular endothelial growth factor (VEGF) production, suggesting an ANXA3-VEGF mediated form of angiogenesis. Subsequent studies further linked *ANXA3* to EC migratory properties and VEGF regulated angiogenesis: *ANXA3* siRNA-treated HUVECs showed reduced migration ability in wound-healing assays,[16] while proteomic studies on VEGF stimulated HUVECs revealed an induction of ANXA3 levels.[27] *in vivo* work in *Xenopus laevis* demonstrated that depletion of Anxa3 results in defective embryonic vascular development characterized by disrupted vessel morphogenesis.[16] However, it remains unclear whether Anxa3 has a prominent *in vivo* role in mammalian vascular development. Therefore, we created *Anxa3* conditional loxP mice and genetically ablated *Anxa3* specifically in the EC lineage to determine its function in mammalian vascular development. We found that *Anxa3* function is not critical to *in utero* blood vessel development, but is necessary for postnatal vascular patterning. Assessment of the murine retina showed that depletion of *Anxa3* in ECs leads to a loss of artery-vein alignment, resulting in vessel crossovers, similar to those that cause

vessel occlusion in humans.[28–30] Overall, these studies indicated a novel role of *Anxa3* in retinal artery-vein patterning.

2 | RESULTS AND DISCUSSION

2.1 | Generation of an Annexin A3 endothelial cell specific knockout mouse

In mice, *Anxa3* is expressed in the embryonic endothelial lineage[16] and is readily detected in adult brain and lung ECs.[17,18] In order to assess the role of *Anxa3* in EC development, we generated mice with *Anxa3* conditional knockout potential using embryonic stem (ES) cell clones designed and purchased from EUCOMM (Figure 1A). *Anxa3* mice were created with loxP sites flanking exon 6 (*Anxa3*$^{f/f}$), which encodes a portion of the second annexin repeat domain involved in calcium binding (Figure 1A). This strategy predicts the loss of ANXA3 protein due to non-sense-mediated decay of the mRNA. *Anxa3*$^{f/f}$ mice were bred into the *Tie2*-Cre mouse line, which express Cre-recombinase in embryonic and adult ECs, and which is commonly used for EC knockout-based mouse studies.[31] DNA assessment of the resulting offspring demonstrated that *Anxa3*$^{f/f}$ and *Anxa3*$^{f/f}$;*Tie2*-Cre mice were readily distinguished by PCR genotyping methods (Figure 1A,B). Furthermore, we found that *Anxa3*$^{f/f}$;*Tie2*-Cre mice were born at Mendelian ratios and survived throughout adulthood (Figure 1C), while exhibiting a normal life expectancy. These results suggested that *Anxa3* is not essential for embryonic vascular development or EC maintenance after birth.

2.2 | Endothelial cell loss of Annexin A3 does not cause embryonic vascular defects

In contrast to our observations, indicating *Anxa3* is dispensable for murine blood vessel development, previous work in *Xenopus laevis* demonstrated that loss of Anxa3 resulted in defective embryonic blood vessel formation.[16] Therefore, to investigate whether any underlying developmental vascular defects were associated with the loss of *Anxa3*, we examined mice at embryonic (E) stage E9.5, which coincides with the completion of initial blood vessels formation (vasculogenesis) and beginning angiogenic growth of new vessels (angiogenesis). *Anxa3*$^{f/f}$ and *Anxa3*$^{f/f}$;*Tie2*-Cre embryos were immunolabeled with antibodies for platelet endothelial cell adhesion molecule (PECAM) and endomucin (EMCN) to reveal all blood vessels within the embryo (Figure 2). In comparison to control *Anxa3*$^{f/f}$ embryos, *Anxa3*$^{f/f}$;*Tie2*-Cre embryos showed no apparent morphological defects in the developing vasculature and no overall changes in embryo size (Figure 2A,B). For instance, the dorsal aorta, intersomitic vessels, and endocardium appeared similar to *Anxa3*$^{f/f}$ embryos (Figure 2A,B). In addition, cross sections of *Anxa3*$^{f/f}$ and *Anxa3*$^{f/f}$;*Tie2*-Cre embryos revealed no gross, obvious defects in size or shape of the dorsal aorta or surrounding blood vessels in *Anxa3* mutants (Figure 2C,D). Moreover, other embryonic structures, such as the notochord, somites, and gut tube appeared normal in shape suggesting no secondary effects on organ formation due to defective blood vessel function (Figure 2C,D). In situ hybridization analysis in *Anxa3*$^{f/f}$ and *Anxa3*$^{f/f}$;*Tie2*-Cre mice demonstrated specific and significant reduction of *Anxa3* transcripts in the endothelium of mutants, although some transcripts consistently remained in the posterior intersomitic vessels (Figure 2E, F). Overall, these observations are consistent with the results showing a lack of embryonic lethality associated with *Anxa3*$^{f/f}$;*Tie2*-Cre mice, and further indicate that *Anxa3* is not required for EC development.

2.3 | Loss of Annexin A3 in retinal endothelial cells leads to an increased number of artery-vein crossovers

To further explore the relationship between *Anxa3* and postnatal vascular development, we used the neonate retina to assess angiogenesis. The retina represents an ideal model to view the developing vasculature due to its flat, two-dimensional like structure, and alternating pattern of arteries and veins that are established after birth.[32–34] *In situ* hybridization for *Anxa3* mRNA was initially performed on postnatal day 7 (P7) retinas to assess its expression in the developing retinal vasculature (Figure 3A). Co-staining with isolectin-IB4, which marks all blood vessels and macrophages, demonstrated that *Anxa3* mRNA was predominately localized to arteries and veins, and to a lesser extent, present in the intervening capillaries of *Anxa3*$^{f/f}$ retinas (Figure 3A,B). In contrast, *Anxa3* transcripts were largely absent in the retinal vasculature of *Anxa3*$^{f/f}$;*Tie2*-Cre mice, indicating efficient genetic ablation of *Anxa3* in retinal ECs (Figure 3C,D). Furthermore, western blot analysis of ECs isolated from P7 lungs demonstrated a significant reduction in levels of ANXA3 in *Anxa3*$^{f/f}$;*Tie2*-Cre mice as compared to *Anxa3*$^{f/f}$ controls (Figure 3E). When comparing *Anxa3*$^{f/f}$ with *Anxa3*$^{f/f}$;*Tie2*-Cre P7 retinas, no angiogenic defects were observed. Peripheral outgrowth of the retinal vasculature showed no statistical difference between *Anxa3*$^{f/f}$ and *Anxa3*$^{f/f}$;*Tie2*-Cre retinas (Figure 3F–H) and vascular densities were unchanged as well (Figure 3F,G,I). Furthermore, the overall morphological appearance of the arteries, veins, and capillaries looked normal (Figure 3F,G). Therefore, *Anxa3* does not appear to play a significant role in regulating angiogenic growth in the retinal vasculature.

However, we noticed artery-vein (AV) alignment defects in many of the P7 *Anxa3*$^{f/f}$;*Tie2*-Cre mutant retinas (Figure 4A,B; insets). Typically, arteries and veins run parallel to each other and remain separated by a capillary bed (Figure 4A). Interestingly, *Anxa3*$^{f/f}$ control retinas displayed atypical AV crossovers (intersection of an artery and vein) approximately 25% of the time (n = 6/23), but multiple AV crossovers were never observed (Figure 4A,C, G). However, when *Anxa3* was deleted in the ECs, we observed a much higher frequency of AV misalignment: 10 out of 16 *Anxa3*$^{f/f}$;*Tie2*-Cre retinas displayed an AV crossover (62.5%) with four retinas having multiple AV crossovers (Figure 4B,C,H). Moreover, *Anxa3*$^{f/f}$;*Tie2*-Cre retinas with multiple AV crossovers often displayed bifurcated veins (Figure 4B,D). Although not statistically significant, this observation was unusual, as bifurcated veins were not observed in *Anxa3*$^{f/f}$ control retinas (Figure 4A, D). Interestingly, in regards to vessel sizes, vein diameters, but not artery diameters, were slightly increased in *Anxa3* mutant retinas (Figure 4A,B,E,F), further suggesting that the veins were more impacted overall by the loss of *Anxa3*. We also noted that in both *Anxa3*$^{f/f}$ and *Anxa3*$^{f/f}$;*Tie2*-Cre retinas with AV crossovers, arteries always intersected over top of veins (Figure 4G–I), similar to patients with BRVO. Taken together, we concluded that *Anxa3* facilitates proper vascular patterning in the retina by maintaining parallel AV alignment.

2.4 | Retinal AV crossovers caused by endothelial loss of Annexin A3 persist into adulthood

To address whether loss of AV alignment persisted throughout adulthood, we collected *Anxa3*$^{f/f}$ and *Anxa3*$^{f/f}$;*Tie2*-Cre retinas from 4- to 9-month-old mice and viewed the vasculature with the EC marker isolectin-IB4. In addition, retinas were costained with

antibodies that detected alpha smooth muscle actin (αSMA) to differentiate arteries from veins, as αSMA expressing cells predominately surround the retinal arteries. (Figure 5A,B) Approximately, 12.5% of control *Anxa3*$^{f/f}$ retinas displayed AV crossovers (n = 2/16) with one retina having two AV crossovers (Figure 5A,C,D).This number of AV crossovers was a reduction in half of those observed at P7 (25%; Figure 4C) indicating a decreased persistence of AV crossovers in control retinas. In contrast, 58% of *Anxa3*$^{f/f}$; *Tie2*-Cre adult retinas were observed to have AV crossovers (n = 7/12; Figure 5B,C,E), which is similar to the number of AV crossovers seen in the P7 retinas (62.5%). Of the seven mice with AV crossovers, three exhibited multiple crossovers in the retina (Figure 5B,C,E). Together, these data provide evidence that defective AV alignment persists in *Anxa3* mutant mice throughout adulthood.

We also point out that in both P7 and adult *Anxa3* control and mutant retinas, AV misalignments happened in all areas of the retina, including both proximal and distal to the optic nerve (Figures 4B,G,H and 5B,D,E). These observations indicated that AV crossovers were not specifically localized in *Anxa3*$^{f/f}$;*Tie2*-Cre retinas. In addition, the distribution in the number of AV crossovers identified in *Anxa3*$^{f/f}$ and *Anxa3*$^{f/f}$;*Tie2*-Cre males and females was not significantly different suggesting there is no link between sex and *Anxa3*-associated AV crossovers (data not shown).

2.5 | Blood vessels associated with AV crossovers show no apparent occlusion

In patients with BRVO, AV crossovers often lead to occlusion of blood flow in the underlying vein due to compression by the artery. To investigate whether blood is occluded from flowing past AV crossovers, the vasculature of both P7 and adult *Anxa3*$^{f/f}$;*Tie2*-Cre retinas was examined for the presence and location of red blood cells. *In situ* hybridization analysis for hemoglobin alpha, adult chain 1 *(Hba-a1)* mRNA, coupled with isolectin-IB4 immunofluorescent labeling, demonstrated that red blood cells were readily detected in the veins and arteries past the AV crossover points of P7 neonate retinas (Figure 6A). This included red blood cells that traveled in arteries peripherally past, and in veins centrally past, the AV crossover (blood flows towards the periphery in arteries and returns in veins towards the optic center in retinas). Similarly, in *Anxa3* mutant adult retinas, TER-119 positive erythrocytes were observed in the veins past the AV crossovers (Figure 6B). Thus, red blood cells do not appear to be impeded or occluded from passing the AV crossovers in *Anxa3*$^{f/f}$;*Tie2*-Cre retinas.

2.6 | RNA-sequencing studies reveal potential genes associated with Anxa3 related AV crossovers

To uncover genes affected by the loss of *Anxa3,* which could potentially be associated with AV crossovers, we performed RNA-sequencing experiments on isolated retinal endothelial cells (iREC) from *Anxa3*$^{f/f}$ and *Anxa3*$^{f/f}$; *Tie2*-Cre P7 pups. These data confirmed that *Anxa3* is down regulated in iRECs, and expression of *Sortilin Related VPS10 Domain Containing Receptor 2 (Sorcs2)* and *Zinc finger FYVE-type containing 28 (Zfyve28)* were also reduced (Table 1). The only up-regulated transcript was *Ubiquitin B* (*ubb*). Given that Annexin proteins are thought to mainly play roles in membrane associated cellular processes, it was not overly surprising to find few transcriptionally misregulated genes in

Anxa3$^{f/f}$;*Tie2*-Cre retinas. However, these genes may represent a starting point for further investigations into their possible roles in AV misalignment phenotypes.

3 | EXPERIMENTAL PROCEDURES

3.1 | Animals

ES cell clones with *Anxa3* conditional deletion potential (Figure 1A) were purchased from EUCOMM (Anxa3$^{tm1a(EUCOMM)Hmgu}$), and loxP sites were sequenced verified. ES cell clones were injected into C57BL/6J blastocysts and subsequent founder mice were identified via PCR genotyping. ROSA26::FLPe knock-in mice (Jackson Laboratory), which ubiquitously express the FLP1 recombinase, were utilized to recombine the FRT sites and remove the *lacZ* and *neomyocin* casettes, and the intervening loxP site. PCR genotyping primers P1 and P2 (see genotyping section) were used to verify FRT recombination. The resulting mice, which contained an *Anxa3* allele with loxP sites flanking (flox, f) exon 6 of the gene and a wild-type *Anxa3* allele (*Anxa3*$^{f/WT}$), were then interbred to create a homozygous *Anxa3* loxP conditional mouse lacking the ROSA26::FLPe knock-in allele (*Anxa3*$^{f/f}$). *Anxa3*$^{f/f}$ and *Tie2*-Cre mice[31] were bred together to create *Anxa3*$^{f/f}$;*Tie2*-Cre mice with *Anxa3* deleted specifically in ECs. *In situ* hybridization and western blot analysis was performed on *Anxa3*$^{f/f}$;*Tie2*-Cre embryonic day 9 (E9.5) embryos and postnatal day 7 (P7) retinas to verify EC-specific loss of *Anxa3* transcripts and protein (Figures 2 and 3). All animal experiments were performed in accordance with Tulane University's Institutional Animal Care and Use Committee policy.

3.2 | Genotyping

Genotyping was performed as previously described.[46] Primers were as follows: Anxa3 forward (P1) 5′-TTGGATGGATGAGTTCAGTGGTAG-3′, Anxa3 reverse (P2) 5′-GACACTAGGTTTCTGATTTTCCGTGC-3′, Anax3 knockout reverse (P3) 5′-TGAACTGATGGCGAGCTCAGACC-3′, Cre forward 5′-G ATCGCTGCCAGGATATACG-3′, Cre reverse 5′-CATCGCC ATCTTCCAGCAG-3′. Wild-type PCR product (P1,P2) = 504 bp ; Mutant loxP PCR product (P1,P2) = 620 bp ; Mutant KO PCR product (P1,P3) = 370 bp (no product for wild type); Cre PCR product = 572 base pairs.

3.3 | Embryo and retina dissections

Embryonic stages were determined via vaginal plug, which was designated as embryonic day 0.5. Embryos were dissected from adult mice at embryonic day 9.5. To ensure that compared embryos were at similar stages, somites were counted. Embryos were fixed in 4% paraformaldehyde (PFA) overnight at 4 C, then dehydrated in a stepwise fashion using an ethanol series, and stored in 75% ethanol at −20 C until needed for staining. For retina collection, eyeballs were dissected from mice at P7 or 2 to 3 months of age and fixed in 4% PFA for 1 hour. After fixation, the retinas were dissected from the eyes, dehydrated in a stepwise fashion, and stored in 75% ethanol at −20 C until use for staining.

3.4 | Embedding and sectioning of embryos

Dehydrated embryos were placed into two subsequent 100% ethanol washes for 10 minutes each. The embryos were then washed with xylenes twice for 5 minutes each. Embryos were then placed into a 50% xylene, 50% paraffin mixture for 30 minutes at 65 C, followed by six 30-minute paraffin washes at 65 C. Embryos were then positioned and moved to a cold plate.

3.5 | Immunofluorescent Staining: whole embryos, embryo sections, and retinas

Whole embryos and embryo sections were rehydrated and washed with PBS. They were then permeabilized for one hour in 1% triton-X in PBS. Before staining, samples were blocked using CAS-block (Invitrogen) for 30 minutes at room temperature. Primary antibodies were diluted 1:100 in CAS-block with 0.5% Triton-X overnight at 4 C. Primary antibodies were as follows: PECAM (BD 553370), ENDOMUCIN (Santa Cruz 6415), and TER-119 (Abcam, ab91113). For sections, DAPI was also used according to manufacturer instructions (Life Technologies R37606). Embryos were then incubated in secondary antibody for 4 hours at room temperature (Lifetech 1907302). Embryos were mounted on a cover-slip in PBS for visualization. All images were taken using Nikon A1 confocal microscope. Retinas were rehydrated in a stepwise fashion, washed with PBS, and placed into PBS +1% Triton (PBST) for 30 minutes to permeabilize. Retinas were then blocked with CAS-Block (Invitrogen) for 30 minutes at room temperature and placed into 1% PBST with primary antibodies (1:200) overnight at 4°C. The retinal stains were as follows: Isolectin-IB4-Alexa Fluor 488 (Invitrogen 21 411) and αSMA-Cy3 (Sigma C6198). Retinas were then washed with PBS and mounted onto slides using Prolong Diamond antifade mountant (Invitrogen). Images were taken on a Nikon A1 confocal microscope (immunofluorescent images) or Leica M205 FA Stereomicroscope (in situ hybridization images with fluorescence).

3.6 | In situ hybridization and expression analysis

In situ hybridization was performed as previously described.[34] Digoxigenin-labeled antisense RNA probes for *Anxa3* were generated as previously described.[16] To make *Hba-a1* antisense RNA, the full-length *Hba-a1* clone (Dharmacon, MMM1010-202858759) was digested with EcoRI restriction enzyme, purified, and transcribed with T3 polymerase. Data for chicken *ANXA1, 10,* and *11* were retrieved from the GEISHA database, University of Arizona, Tucson, AZ; URL: http://geisha.arizona.edu; [7/16/2019]. Expression analysis of mouse, annexins used single cell RNA-sequencing data obtained from ECs isolated from adult brain and lung: http://betsholtzlab.org/VascularSingleCells/database.html. Retinas were imaged using a Leica M205 FA stereomicroscope.

3.7 | Image analysis

All retinal images were analyzed using Nikon NIS-Elements AR analysis 64-bit software or ImageJ. Retinal outgrowth was measured by taking three measurements from the optic nerve to the outermost vascular periphery per retina. Retinal vascular densities were measured using a macro on the ImageJ software. Three areas containing an artery, vein, and intervening capillaries were measured per retina to calculate vascular density. Venous and

arterial diameters were determined using the ImageJ software: three veins and three arteries from each retina were measured at their widest points and used to quantify vessel diameters. The number of crossovers and the number of arteries and veins were counted manually using whole retina images.

3.8 | Statistical analysis

All statistics and graphs were generated using GraphPad Prism software. Two-tailed Student's *t*-tests with Welch's correction were used to compare between *Anxa3*$^{f/f}$ and *Anxa3*$^{f/f}$;*Tie2*-Cre groups. A *P* value of <.05 was considered significant.

3.9 | RNA extraction

RNA from retinal and lung ECs were isolated as previously described.[47] Briefly, freshly dissected tissues were minced and placed in collagenase I (Gibco 17 100-017)-dispase (Corning 354 235) solution for 30 minutes at 37°C, and passed through a cannula to obtain a single cell suspension. The single cell suspension was then centrifuged at 2000 x g and the supernatant removed. The pellet was resuspended in isolation buffer, filtered over a 0.70 μm nylon mesh filter and incubated with CD31 (BD 553370) conjugated dynabeads for 20 minutes at room temperature. The dynabead mixture was washed five times in isolation buffer before RNA or protein isolation. For RNA purification, lysis buffer containing beta-mercaptoethanol was added to the dynabead mixture and vortexed, followed by the addition of 100% ethanol. The dynabead mixture was placed on a magnet to remove beads and the remaining lysate was subjected to RNA purification. We used the Thermo Fisher GeneJET RNA Purification kit (Thermo #K0732) and quantified RNA via nanodrop (Thermo) and Qubit (Thermo Q33216).

3.10 | RNA-sequencing, analysis, and access

RNA quality was assessed using the Agilent RNA 6000 Nanokit (Agilent 5067-1511) before library preparation. Libraries were constructed using Illumina TruSeq RNA Library Preparation Kit v2 (Illumina RS-122-2001). Quality and quantity of the library were assessed using Agilent DNA 1000 chip (Agilent 5067-1504) and Qubit dsDNA HS Kit (Thermo Q32854), respectively. Libraries were sequenced on MiSeq (Illumina). Alignment was performed using Basespace RNA-Seq aligner (v1.1.0) and differential expression analysis was performed using Basespace DESeq2 (v1.1.0). RNA-seq data is available on the National Center for Biotechnology Information's GEO database (https://www.ncbi.nlm.nih.gov/geo/browse/). Accession number (GSE135528).

3.11 | Western blot

Protein was extracted from isolated lung ECs using RIPA buffer (Thermo 89 900) supplemented with protease inhibitor (Thermo 78 430). Proteins concentration was assessed using a BCA protein assay kit (Thermo 23 225). Proteins were separated by SDS-PAGE and blotted onto nitrocellulose membranes. Membranes were probed with specific primary antibodies and then with fluorescently labeled secondary antibodies. The following primary antibodies were used: Anxa3 (Sigma HPA013431, 1:1000), β-Actin (Cell signaling 3700,

1:5000). The bands were visualized using an Odyssey imaging system (LI-COR Biosciences).

4 | CONCLUSIONS

The parallel alignment of arteries and veins is critical for proper blood flow and vessel function. For example, when blood vessels become misaligned in the mouse skin, the animal is unable to thermoregulate as efficiently, causing an increase in body temperature that can lead to heat stroke.[35] In patients with branch retinal vein occlusion (BRVO), the inappropriate intersection of retinal arteries on top of veins can cause changes in blood flow within the vein and result in occlusion of the underlying vein.[28–30] As a consequence, these patients often experience dramatic vision loss.[36] In terms of genetic animal studies, few AV misalignment phenotypes, such as AV crossovers, have been described in the retina. In 2003, retinal AV crossover points were reported in hemizygous mice lacking *Vegf-A* in neuronal progenitor cells.[37] In support of this observation, increased numbers of retinal AV crossings were identified in P28 mice treated with the VEGF receptor tyrosine kinase inhibitor KRN633 at P0 and P1.[38] In addition, mice expressing a form of Neuropilin-1 (NRP1) that lacks the cytoplasmic domain exhibit an increased incidence of retinal AV crossovers.[39] Since NRP1 can serve as a receptor for VEGF-A,[40] these data suggest that VEGF-NRP1 signaling may play a prominent role in retinal AV patterning. Interestingly, several *in vitro* studies link the expression levels of ANXA3 and VEGF: overexpression of *ANXA3* in HEK 293 cells leads to increased production of VEGF in the cultured media,[26] while stimulation of HUVECs with VEGF leads to higher levels of ANXA3.[27] Therefore, a potential VEGF-NRP1-ANXA3 signaling axis may regulate AV parallel alignment.

In an attempt to identify pathways and factors related to *Anxa3* regulation of AV crossovers, we performed RNA-sequencing analysis on iRECs from *Anxa3* mutant retinas. This study revealed that *Sorcs2* and *Zfyve28* were down regulated in the absence of *Anxa3*. Although neither genes have been shown to be explicitly expressed in the EC lineage, it is noteworthy that overexpression of ZFYVE28 in cultured podocytes promotes Epidermal Growth Factor (EGF) signaling,[41] which is tied to VEGF signaling and has been shown to increase VEGF production during tumor-angiogenesis and angiogenesis.[42] On the other hand, there is no apparent connection between *Sorcs2* and AV patterning since *Sorcs2* is predominately associated with neuronal viability and signaling.[43,44] A potential link with both *Sorcs2* and *Zfyve28* could be tied to the interaction between the neural astrocytes and ECs in the retina; the underlying astrocytes express VEGF and control blood vessel pattering in the retina.[45] However, how loss of *Sorcs2* and *Zfyve28* in the context of the ECs effects AV crossovers remains to be seen and indicates that more studies are needed to determine if either factor is involved in regulation of AV alignment.

Overall, our studies provide evidence of a novel role for Anxa3 in preventing retinal AV crossovers in mammals. In further support of these data, mousephenotype.org reports that adult homozygous *Anxa3* null mice exhibit significant phenotypes only in the eye, namely abnormal lens morphology, and retinal blood vessel pattern defects. Although not described in detail, we propose that the AV crossovers and vein bifurcations identified in *Anxa3*$^{f/f}$; *Tie2*-Cre retinas could be indicative of the observed retinal vascular patterning defects seen

in *Anxa3* null mice. Furthermore, the *Anxa3* null mice are viable at adulthood suggesting relatively normal vascular development, similar to our results (Figure 2). However, unlike patients with BRVO, *Anxa3* related retinal AV crossovers did not lead to occluded vessels suggesting that other factors may be required and involved, and that loss of *Anxa3* may be a first step in a series of changes that must occur to lead to vein occlusion. Future studies aimed at identifying the genetic factors involved in human retinal diseases, such as BRVO, will be important for revealing the potential contributions of ANXA3, VEGF, and NRP1 in vessel patterning defects.

ACKNOWLEDGMENTS

This work was supported by a Tulane University Carol Lavin Bernick Faculty Grant (S.M.M.), Tulane University start-up funds (S.M.M.), and NIH HL113498 (O.C.). We would like to thank the UT Southwestern Medical Center transgenic core for performing *Anxa3* ES cell injections; EUCOMM for the *Anxa3* mutant ES cells; Jovanny Zabaleta and Jone Garai at Lousiana State University Health Sciences Research Center for their expertise and guidance on next generation sequencing studies; Melody C. Baddoo with the Tulane Cancer Center Cancer Crusaders Next Generation Sequence (NGS) Analysis Core for assistance with RNA-Seq analysis. The NGS Analysis core is supported by the National Institutes of Health National Cancer Institute, Award Number P01CA214091. The content is solely the responsibility of the authors and does not necessarily represent the official views of the National Institutes of Health.

Funding information

National Heart, Lung, and Blood Institute, Grant/Award Number: HL113498; National Institutes of Health; National Institutes of Health National Cancer Institute, Grant/Award Number: P01CA214091; UT Southwestern Medical Center; Tulane University Carol Lavin Bernick Faculty Grant

REFERENCES

1. Gerke V, Creutz CE, Moss SE. Annexins: linking Ca^{2+} signalling to membrane dynamics. Nat Rev Mol Cell Biol. 2005;6(6): 449–461. [PubMed: 15928709]
2. Myrvang HK, Guo X, Li C, Dekker LV. Protein interactions between surface annexin A2 and S100A10 mediate adhesion of breast cancer cells to microvascular endothelial cells. FEBS Lett. 2013;587(19):3210–3215. [PubMed: 23994525]
3. Ali SM, Geisow MJ, Burgoyne RD. A role for calpactin in calcium-dependent exocytosis in adrenal chromaffin cells. Nature. 1989;340(6231):313–315. [PubMed: 2526299]
4. Gruenberg J, Stenmark H. The biogenesis of multivesicular endosomes. Nat Rev Mol Cell Biol. 2004;5(4):317–323. [PubMed: 15071556]
5. Hayes MJ, Rescher U, Gerke V, Moss SE. Annexin-actin interactions. Traffic. 2004;5(8):571–576. [PubMed: 15260827]
6. Futter CE, White IJ. Annexins and endocytosis. Traffic. 2007;8 (8):951–958. [PubMed: 17547702]
7. Martin-Belmonte F, Gassama A, Datta A, et al. PTEN-mediated apical segregation of phosphoinositides controls epithelial morphogenesis through Cdc42. Cell. 2007;128(2):383–397. [PubMed: 17254974]
8. Datta A, Bryant DM, Mostov KE. Molecular regulation of lumen morphogenesis. CurrBiol. 2011;21(3):R126–R136.
9. Boye TL, Jeppesen JC, Maeda K, et al. Annexins induce curvature on free-edge membranes displaying distinct morphologies. Sci Rep. 2018;8(1):10309. [PubMed: 29985397]
10. Dreier R, Schmid KW, Gerke V, R K. Differential expression of annexins I, II, and IV in human tissues: an immunohistochemical study. Histochem Cell Biol. 1998;110(2):137–148. [PubMed: 9720986]
11. Brachvogel B, Welzel H, Moch H, von der mark K, Hofmann C, Poschl E. Sequential expression of annexin A5 in the vasculature and skeletal elements during mouse development. Mech Dev. 2001;109(2):389–393. [PubMed: 11731255]

12. Farber SA, De Rose RA, Olson ES, Halpern ME. The zebrafish annexin gene family. Genome Res. 2003;13(6A):1082–1096. [PubMed: 12799347]
13. Ling Q, Jacovina AT, Deora A, et al. Annexin II regulates fibrin homeostasis and neoangiogenesis in vivo. J Clin Investig. 2004; 113(1):38–48. [PubMed: 14702107]
14. Darnell DK, kaur S, Stanislaw S, et al. GEISHA: an in situ hybridization gene expression resource for the chicken embryo. Cytogenet Genome Res. 2007;117(1–4):30–35. [PubMed: 17675842]
15. Pin AL, Houle F, Fournier P, et al. Annexin-1-mediated endothelial cell migration and angiogenesis are regulated by vascular endothelial growth factor (VEGF)-induced inhibition of miR-196a expression. J Biol Chem. 2012;287(36):30541–30551. [PubMed: 22773844]
16. Meadows SM, Cleaver O. Annexin A3 regulates early blood vessel formation. PLoS One. 2015;10(7):e0132580. [PubMed: 26182056]
17. He L, Vanlandewijck M, Mae MA, et al. Single-cell RNA sequencing of mouse brain and lung vascular and vessel-associated cell types. Sci Data. 2018;5:180160. [PubMed: 30129931]
18. Vanlandewijck M, He L, Mae MA, et al. A molecular atlas of cell types and zonation in the brain vasculature. Nature. 2018; 554(7693):475–480. [PubMed: 29443965]
19. Huang B, Deora AB, He KL, et al. Hypoxia-inducible factor-1 drives annexin A2 system-mediated perivascular fibrin clearance in oxygen-induced retinopathy in mice. Blood. 2011;118 (10):2918–2929. [PubMed: 21788340]
20. Madureira PA, Surette AP, Phipps KD, Taboski MA, Miller VA, Waisman DM. The role of the annexin A2 heterotetramer in vascular fibrinolysis. Blood. 2011;118(18):4789–4797. [PubMed: 21908427]
21. Knop M, Aareskjold E, Bode G, Gerke V. Rab3D and annexin A2 play a role in regulated secretion of vWF, but not tPA, from endothelial cells. EMBO J. 2004;23(15):2982–2992. [PubMed: 15257287]
22. Brandherm I, Disse J, Zeuschner D, Gerke V. cAMP-induced secretion of endothelial von Willebrand factor is regulated by a phosphorylation/dephosphorylation switch in annexin A2. Blood. 2013;122(6):1042–1051. [PubMed: 23757730]
23. Su SC, Maxwell SA, Bayless KJ. Annexin 2 regulates endothelial morphogenesis by controlling AKT activation and junctional integrity. J Biol Chem. 2010;285(52):40624–40634. [PubMed: 20947498]
24. Raddum AM, Evensen L, Hollas H, Grindheim AK, Lorens JB, Vedeler A. Domains I and IV of annexin A2 affect the formation and integrity of in vitro capillary-like networks. PLoS One. 2013;8(3):e60281. [PubMed: 23555942]
25. Luo M, Flood EC, Almeida D, et al. Annexin A2 supports pulmonary microvascular integrity by linking vascular endothelial cadherin and protein tyrosine phosphatases. J Exp Med. 2017; 214(9):2535–2545. [PubMed: 28694388]
26. Park JE, Lee DH, Lee JA, et al. Annexin A3 is a potential angiogenic mediator. Biochem Biophys Res Commun. 2005;337 (4):1283–1287. [PubMed: 16236264]
27. Mohr T, Haudek-Prinz V, Slany A, Grillari J, Micksche M, Gerner C. Proteome profiling in IL-1beta and VEGF-activated human umbilical vein endothelial cells delineates the interlink between inflammation and angiogenesis. PLoS One. 2017;12(6): e0179065. [PubMed: 28617818]
28. Weinberg D, Dodwell DG, Fern SA. Anatomy of arteriovenous crossings in branch retinal vein occlusion. Am J Ophthalmol. 1990;109(3):298–302. [PubMed: 2309862]
29. Zhao J, Sastry SM, Sperduto RD, Chew EY, Remaley NA. Arteriovenous crossing patterns in branch retinal vein occlusion. The Eye Disease Case-Control Study Group. Ophthalmology. 1993;100(3):423–428. [PubMed: 8460014]
30. Weinberg DV, Egan KM, Seddon JM. Asymmetric distribution of arteriovenous crossings in the normal retina. Ophthalmology. 1993;100(1):31–36. [PubMed: 8433824]
31. Kisanuki YY, Hammer RE, Miyazaki J, Williams SC, Richardson JA, Yanagisawa M. Tie2-Cre transgenic mice: a new model for endothelial cell-lineage analysis in vivo. Dev Biol. 2001;230(2):230–242. [PubMed: 11161575]
32. Fruttiger M Development of the mouse retinal vasculature: angiogenesis versus vasculogenesis. Invest Ophthalmol Vis Sci. 2002;43(2):522–527. [PubMed: 11818400]

33. Fruttiger M Development of the retinal vasculature. Angiogenesis. 2007;10(2):77–88. [PubMed: 17322966]
34. Crist A, Young C, Meadows SM. Characterization of arteriovenous identity in the developing neonate mouse retina. Gene Expr Patterns. 2017;23–24:22–31.
35. Kidoya H, Naito H, Muramatsu F, et al. APJ regulates parallel alignment of arteries and veins in the skin. Dev Cell. 2015;33 (3):247–259. [PubMed: 25920569]
36. Cahill MT, Fekrat S. Arteriovenous sheathotomy for branch retinal vein occlusion. Ophthalmol Clin North Am. 2002;15:417–423. [PubMed: 12515073]
37. Haigh JJ, Morelli PI, Gerhardt H, et al. Cortical and retinal defects caused by dosage-dependent reductions in VEGF-A paracrine signaling. Dev Biol. 2003;262(2):225–241. [PubMed: 14550787]
38. Morita A, Sawada S, Mori A, et al. Establishment of an abnormal vascular patterning model in the mouse retina. J Pharmacol Sci. 2018;136(4):177–188. [PubMed: 29627228]
39. Fantin A, Schwarz Q, Davidson K, Normando EM, Denti L, Ruhrberg C. The cytoplasmic domain of neuropilin 1 is dispensable for angiogenesis, but promotes the spatial separation of retinal arteries and veins. Development. 2011;138(19):4185–4191. [PubMed: 21852397]
40. Lampropoulou A, Ruhrberg C. Neuropilin regulation of angiogenesis. Biochem Soc Trans. 2014;42(6):1623–1628. [PubMed: 25399580]
41. Zambrano S, Rodriguez PQ, Guo J, Moller-Hackbarth K, Schwarz A, Patrakka J. FYVE domain-containing protein ZFYVE28 regulates EGFR-signaling in podocytes but is not critical for the function of filtration barrier in mice. Sci Rep. 2018;8(1):4712. [PubMed: 29549365]
42. Larsen AK, Ouaret D, El Ouadrani K, Petitprez A. Targeting EGFR and VEGF(R) pathway cross-talk in tumor survival and angiogenesis. Pharmacol Ther. 2011;131(1):80–90. [PubMed: 21439312]
43. Glerup S, Olsen D, Vaegter CB, et al. SorCS2 regulates dopaminergic wiring and is processed into an apoptotic two-chain receptor in peripheral glia. Neuron. 2014;82(5):1074–1087. [PubMed: 24908487]
44. Glerup S, Bolcho U, Molgaard S, et al. SorCS2 is required for BDNF-dependent plasticity in the hippocampus. Mol Psychiatry. 2016;21(12):1740–1751. [PubMed: 27457814]
45. Scott A, Powner MB, Gandhi P, et al. Astrocyte-derived vascular endothelial growth factor stabilizes vessels in the developing retinal vasculature. PLoS One. 2010;5(7):e11863. [PubMed: 20686684]
46. Crist AM, Lee AR, Patel NR, Westhoff DE, Meadows SM. Vascular deficiency of Smad4 causes arteriovenous malformations: a mouse model of Hereditary Hemorrhagic Telangiectasia. Angiogenesis. 2018;21(2):363–380. [PubMed: 29460088]
47. Crist AM, Zhou X, Garai J, et al. Angiopoietin-2 inhibition rescues arteriovenous malformation in a Smad4 Hereditary Hemorrhagic Telangiectasia mouse model. Circulation. 2019;139 (17):2049–2063. [PubMed: 30744395]

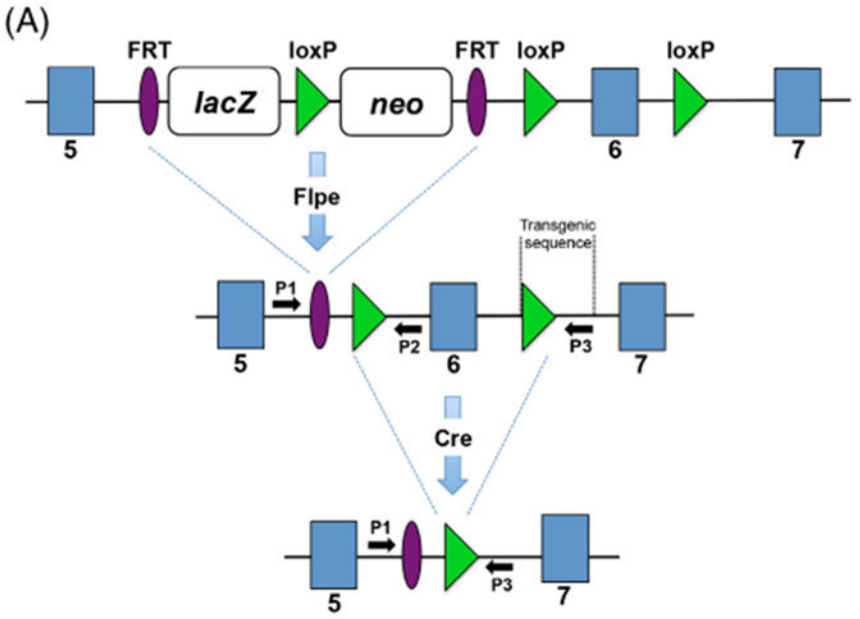

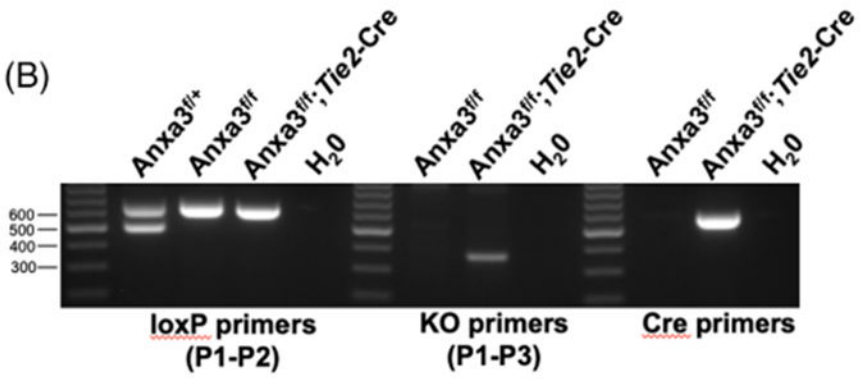

(C)

Numbers of P21 mice obtained from: *Anxa3*$^{f/f}$;*Tie2*-Cre x *Anxa3*$^{f/f}$ matings

Genotype	*Anxa3*$^{f/f}$	*Anxa3*$^{f/f}$;*Tie2*-Cre
Observed mice	129 (52%)	119 (48%)
Expected mice	124 (50%)	124 (50%)

FIGURE 1.

Generation of Annexin A3 endothelial cell-specific knockout mice. A, Graphical representation of strategy used to generate *Anxa3* conditional loxP mice. Flpe recombinase was used to recombine the FRT sites and remove the *lacZ* and *neomyocin (neo)* cassettes, thereby creating *Anxa3* exon 6 flanking loxP (flox) mice termed *Anxa3*$^{f/f}$ (f, flox). Cre recombinase in *Anxa3*$^{f/f}$;*Tie2*-Cre mice results in loxP recombination and deletion of exon 6 in ECs. Exons are indicated by blue boxes. Primer (P1-P3) positions and orientation are indicated by black arrows. Transgenic sequences are unique to the transgenic *Anxa3* allele.

B, Polymerase chain reaction genotyping results. Primers indicated in, A, reveal *Anxa3* mouse genotypes: wild-type *Anxa3* band, 504 bp; *Anxa3* flox band, 620 bp; *Anxa3* knockout (KO) band, 370 bp. C, Table indicates the overall number of *Anxa3*$^{f/f}$ and *Anxa3*$^{f/f}$;*Tie2*-Cre mice at postnatal day 21 (P21). *Anxa3* mutant mice were found at normal Mendelian ratios

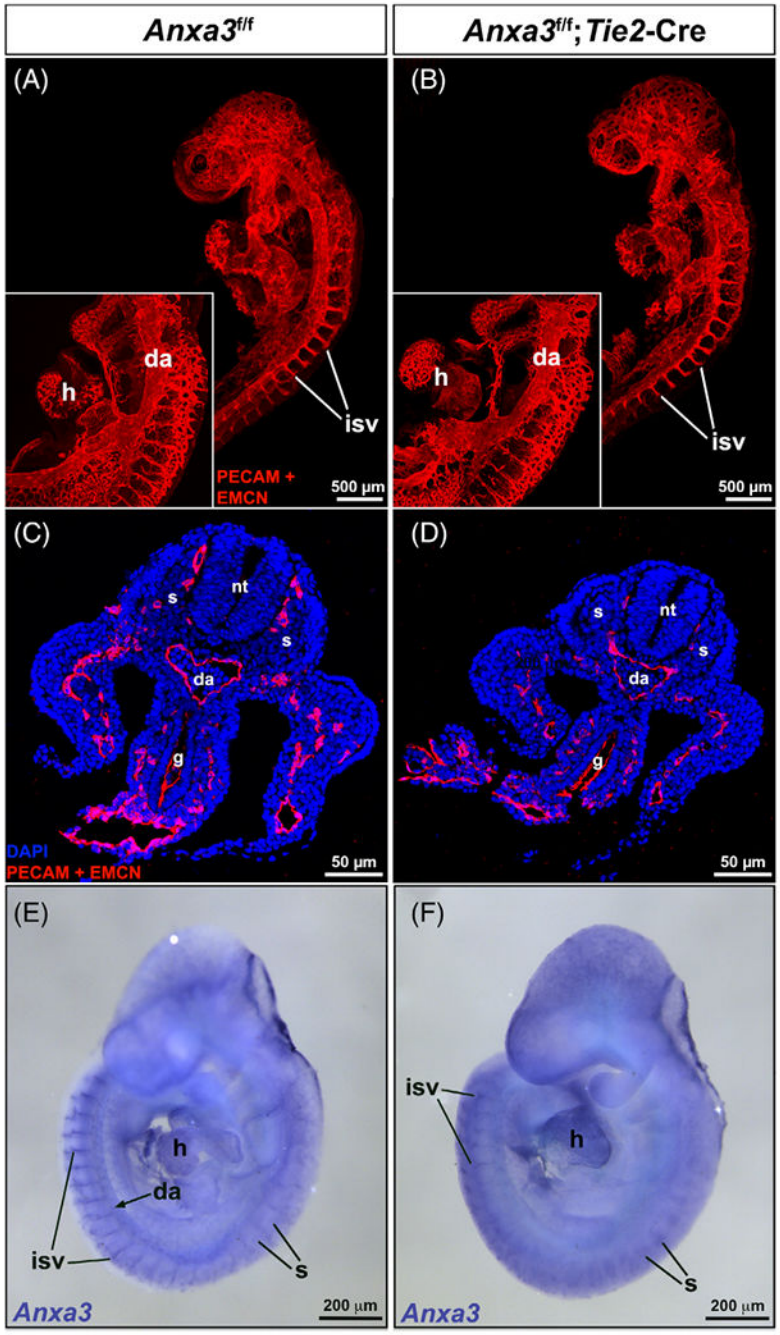

FIGURE 2.

Endothelial cell-specific loss of Annexin A3 does not cause embryonic vascular defects. A,B, *Anxa3*$^{f/f}$ and *Anxa3*$^{f/f}$;*Tie2*-Cre embryonic day 9.5 (E9.5) mouse embryos fluorescently immunolabeled for PECAM and ENDOMUCIN (EMCN) (red) to reveal the embryonic vascular network. No gross morphological defects were observed in the vasculature of *Anxa3*$^{f/f}$;*Tie2*-Cre mutants (n = 6) when compared to *Anxa3*$^{f/f}$ mice (n = 6). da, dorsal aorta; h, heart; isv, intersomitic vessel. C,D, PECAM and ENDOMUCIN (red), and DAPI (blue) immunofluorescent stainings on transverse sections from E9.5 *Anxa3*$^{f/f}$ (n

= 3) and *Anxa3*$^{f/f}$;*Tie2*-Cre (n = 3) embryos. nt, notochord; s, somite; g, gut tube. E,F, In situ hybridization analysis on E9.5 *Anxa3*$^{f/f}$ (n = 3) and *Anxa3*$^{f/f}$; *Tie2*-Cre (n = 3) mice demonstrated a loss of *Anxa3* transcripts in the endothelium of mutants, including reduced expression in the dorsal aorta and intersomitic vessels (notice few *Anxa3* labeled intersomitic vessels in mutants). Note that nonvascular expression of *Anxa3* mRNA in the head region, heart, and somites is retained in *Anxa3* mutant embryos indicating EC-specific inactivation of Anxa3

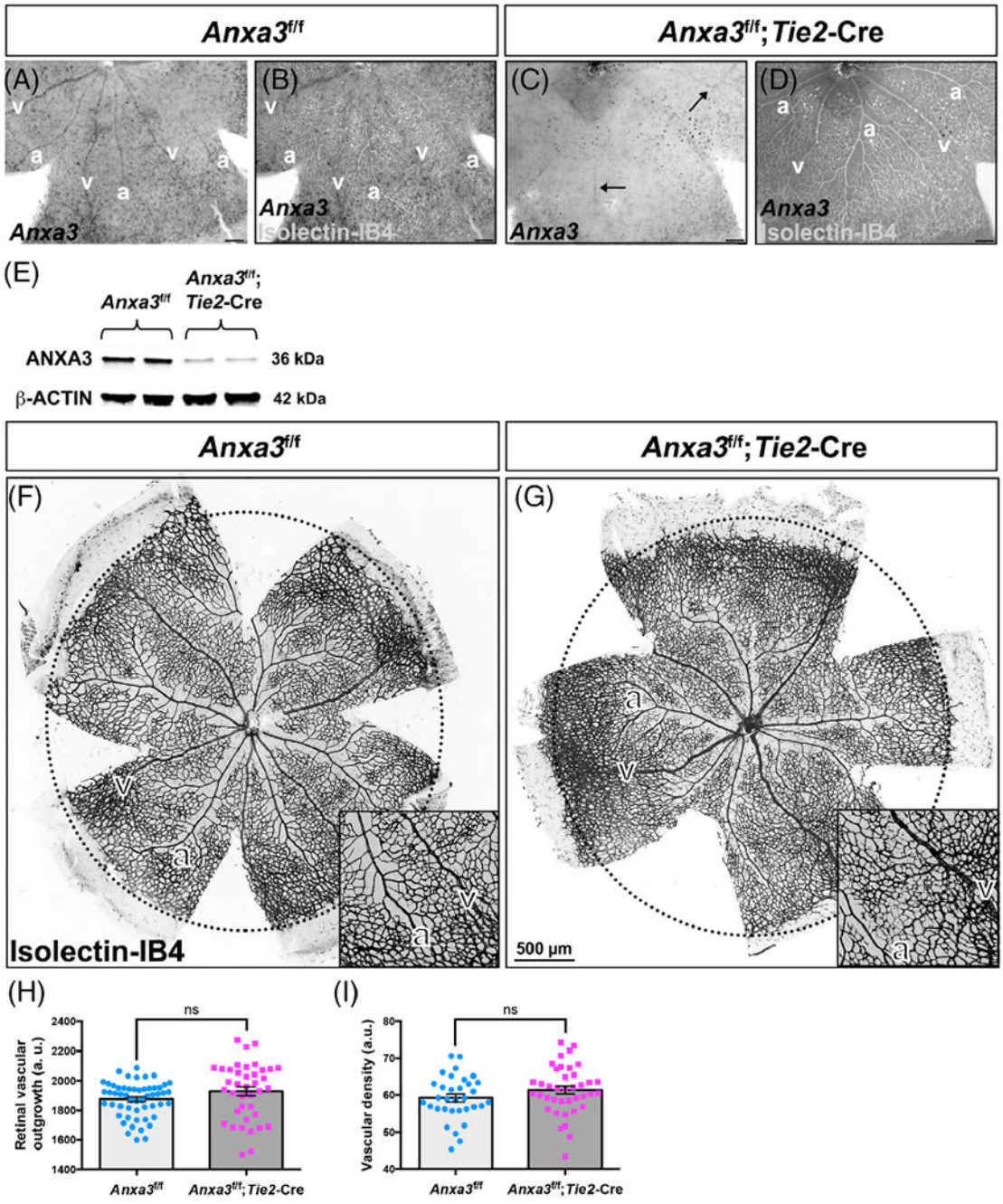

FIGURE 3.

Retinal angiogenesis proceeds normally in the endothelial cell-specific absence of Annexin A3. A-D, Close-up images of postnatal day 7 (P7) *Anxa3*$^{f/f}$ (n = 3) and *Anxa3*$^{f/f}$;*Tie2*-Cre (n = 3) retinas subjected to *in situ* hybridization and immunofluorescent antibody staining. *Anxa3* transcripts (black) are expressed in the vasculature of *Anxa3*$^{f/f}$ retinas, A,B, but are largely absent in *Anxa3*$^{f/f}$;*Tie2*-Cre retinas, C,D, indicating efficient knockdown of *Anxa3.* Black arrows in, C, point to residual *Anxa3* RNA expressed in the vasculature. Isolectin-IB4 immunofluorescent staining (white) marks the entire retinal vascular network and

macrophages. a, artery; v, vein. Scale bars represent 100 pm. E, Western blot analysis of ECs isolated from *Anxa3*$^{f/f}$ and *Anxa3*$^{f/f}$;*Tie2*-Cre P7 lungs showed a significant reduction in levels of ANXA3 protein, indicating that loss of *Anxa3* mRNA corresponds to reduced protein levels. β-ACTIN served as a loading control. F,G, *Anxa3*$^{f/f}$ and *Anxa3*$^{f/f}$;*Tie2*-Cre P7 whole-mount retinas stained for Isolectin-IB4 (black). Loss of *Anxa3* does not influence vascular outgrowth (dotted circles represent the retinal vascular outgrowth of the retina in, E, or vascular density (highlighted by the insets). H,I, Quantification of retinal vascular outgrowth and vascular density in Anxa3$^{f/f}$ (outgrowth, n = 18; density, n = 11) and *Anxa3*$^{f/f}$;*Tie2*-Cre (outgrowth, n = 13; density, n = 13) retinas. Three measurements were taken per retina for quantifying outgrowth and vascular densities (each measurement is depicted on the graph; n represents an individual retina). Statistics were generated using two-tailed Student's *t*-test with Welch's correction. Error bars represent mean ± SEM. ns, not significant; a.u., arbitrary units

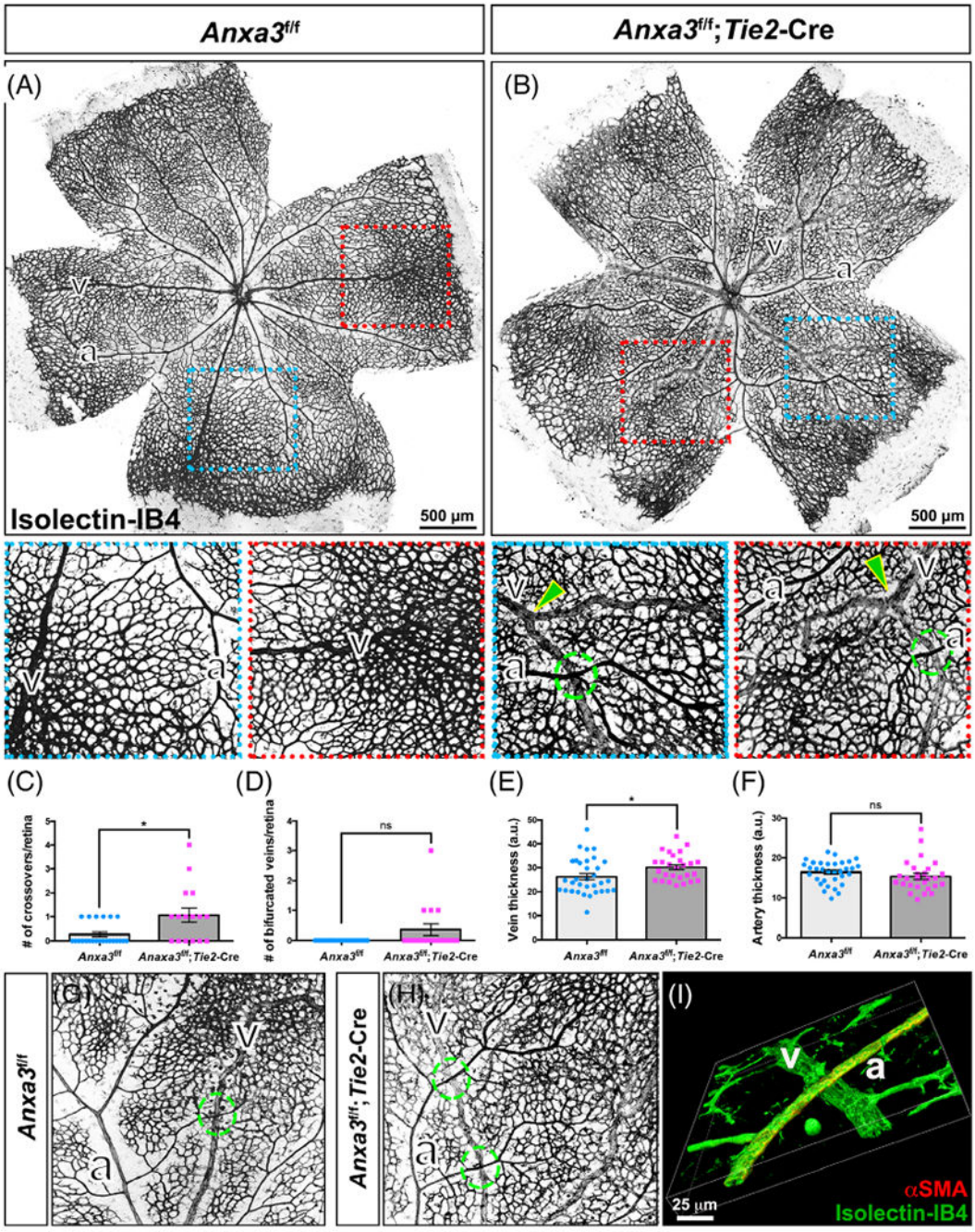

FIGURE 4.

Annexin A3 mutant mice display increased numbers of AV crossovers in P7 retinas. A,B, Postnatal day 7 (P7) *Anxa3*$^{f/f}$ and *Anxa3*$^{f/f}$; *Tie2*-Cre retinas immunofluorescently labeled with Isolectin-IB4 (black). Increased numbers of AV crossovers (green dotted circles) and vein thickness (green/yellow arrows) were observed in *Anxa3* mutant retinas. Notice vein bifurcations are only present in *Anxa3*$^{f/f}$;*Tie2*-Cre retinas. Corresponding close-up insets can be found in red and blue dotted boxes. C-F, Quantifications of AV crossovers, vein bifurcations, and vessel thicknesses in *Anxa3*$^{f/f}$ and *Anxa3*$^{f/f}$; *Tie2*-Cre retinas. Statistics

were generated using two-tailed Student's *t*-test with Welch's correction. Error bars represent mean ± SEM. **P* < .05; ns, not significant; a.u., arbitrary units. C, *Anxa3*$^{f/f}$;*Tie2*-Cre P7 retinas (n = 16) exhibited a statistically significant increase in the number of AV crossovers per retina compared to *Anxa3*$^{f/f}$ control retinas (n = 23). D, No statistical differences were observed in the number of vein bifurcations between *Anxa3*$^{f/f}$;*Tie2*-Cre (n = 16) and *Anxa3*$^{f/f}$(n = 23) retinas, although only *Anxa3* mutants exhibited bifurcated veins. E,F, *Anxa3*$^{f/f}$;*Tie2*-Cre P7 retinas (n = 9) showed statistically significant increases in vein thickness, but no increase in arterial thickness compared to *Anxa3* controls (n = 11). Three veins and three arteries were measured per retina for quantification (each measurement is depicted on the graph; n represents an individual retina). G,H, Close-up views of AV crossovers (dotted green circles) in *Anxa3*$^{f/f}$ and *Anxa3*$^{f/f}$;*Tie2*-Cre retinas stained with Isolectin-IB4. I, 3D reconstruction of an AV crossover in an *Anxa3*$^{f/f}$;*Tie2*-Cre retina fluorescently immunolabeled with Isolectin-IB4 (green) and αSMA (red); an artery (co-stained with αSMA) crosses over a vein, typical of all AV crossovers observed in control and mutant *Anxa3* retinas. a, artery; v, vein

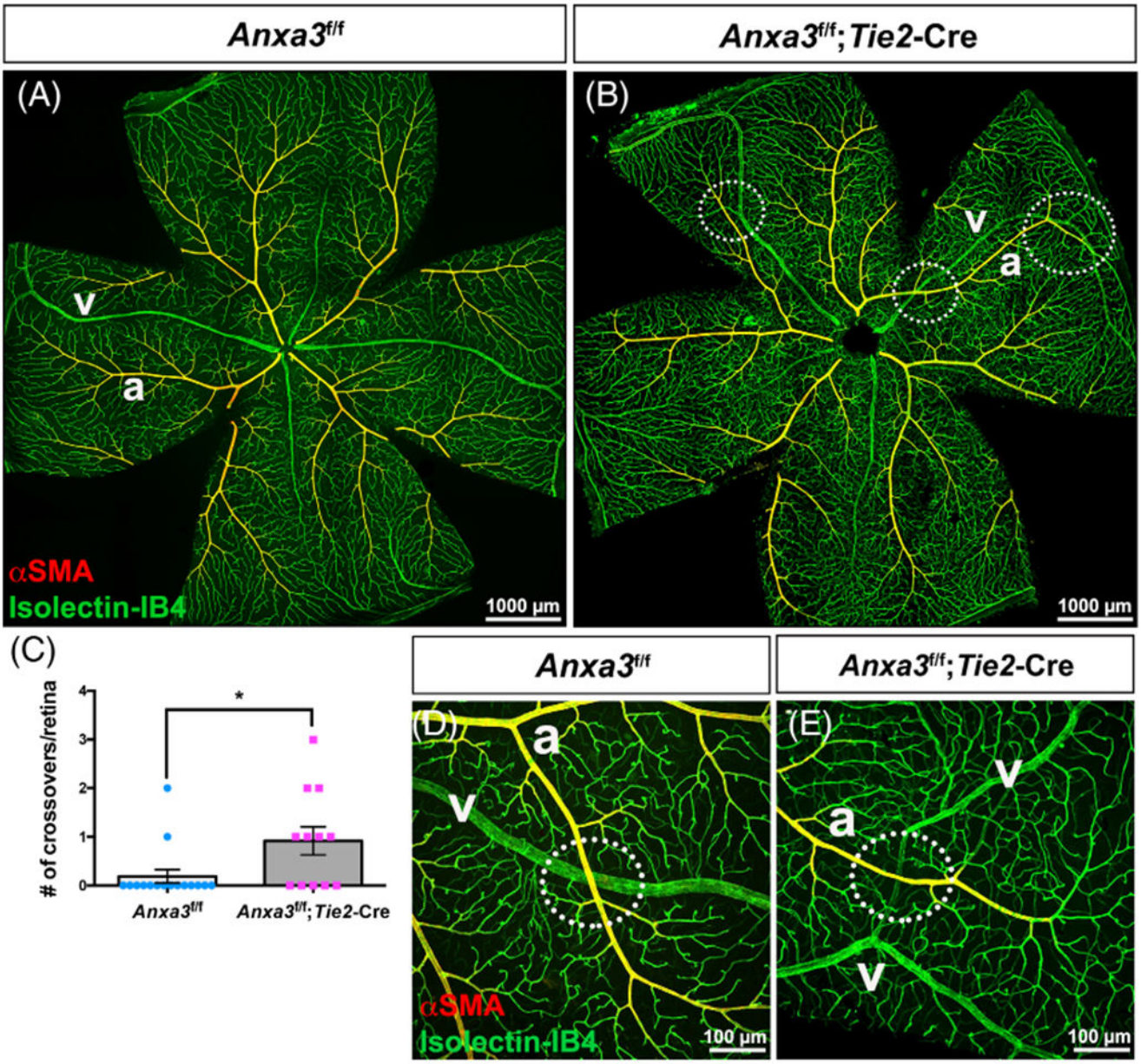

FIGURE 5.

Retinal AV crossovers in Annexin A3 mutant mice persist into adulthood. A,B, Immunofluorescent staining of 4- to 9-month-old *Anxa3*$^{f/f}$ and *Anxa3*$^{f/f}$;*Tie2*-Cre retinas with Isolectin-IB4 (green), which marks the entire retinal vasculature and αSMA (red), which stains smooth muscle cells that only surround arteries. White dotted circles highlight AV crossovers. C, Quantification of AV crossovers show that *Anxa3*$^{f/f}$;*Tie2*-Cre retinas (n = 12) exhibited statistically significant increases in the number of AV crossovers compared to control *Anxa3*$^{f/f}$ retinas (n = 16). Statistics were generated using two-tailed Student's *t*-test with Welch's correction. Error bars represent mean ± SEM. **P* < .05. D,E, Close up images of *Anxa3*$^{f/f}$ and *Anxa3*$^{f/f}$;*Tie2*-Cre adult retinas showing AV crossovers (white dotted circles). a, artery; v, vein

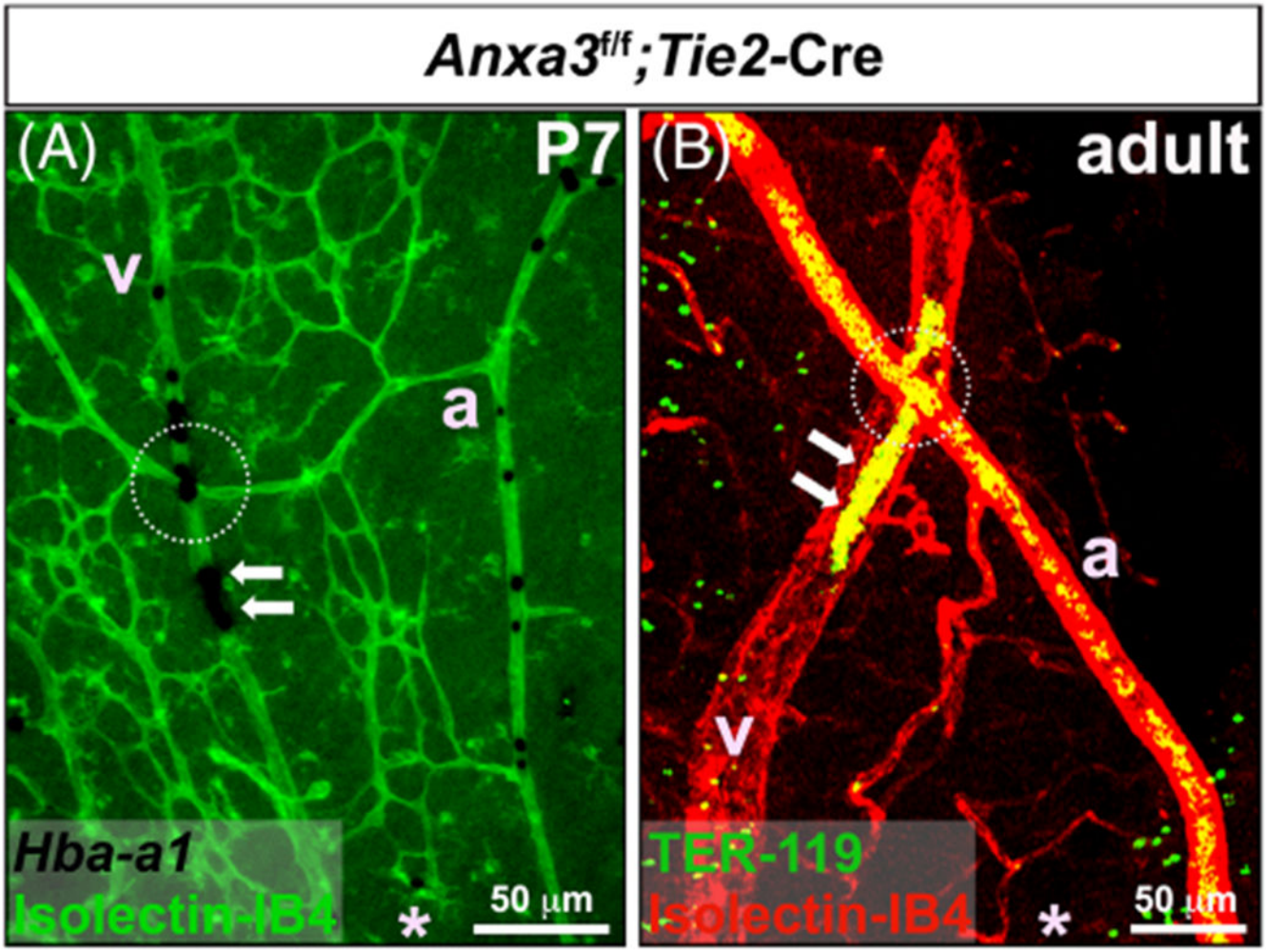

FIGURE 6.

AV crossovers do not lead to occluded blood vessels in Annexin A3 mutant retinas. A, *Anxa3*$^{f/f}$;*Tie2*-Cre P7 retinas (n = 3) subjected to *in situ* hybridization analysis for *Hba-a1* transcripts and immunofluorescent staining for Isolectin-IB4. B, *Anxa3*$^{f/f}$;*Tie2*-Cre 4-9 month old retinas (n = 3) immunofluorescently labeled for Isolectin-IB4 and the erythrocyte marker TER-119. White dotted circles highlight AV crossovers. White arrows point to *Hba-a1* and TER-119 positive red blood cells that have passed the AV crossovers and lie within the corresponding veins (blood flow is towards the optic opening). As a point of reference, the white asterisks denote the direction of the centric optic nerve opening. a, artery; v, vein

TABLE 1

RNA-sequencing results obtained from *Anxa3*$^{f/f}$ and *Anxa3*$^{f/f}$;*Tie2*-Cre isolated retinal endothelial cells (iRECs). Reduced expression of *Anxa3* mRNA confirms deletion in *Anxa3*$^{f/f}$;*Tie2*-Cre retinal ECs

Gene	Log2 fold change
Sorcs2	−0.63
Anxa3	−0.47
Zfyve28	−0.41
Ubb	0.38